Fragility curves for bridges under differential support motions

Konakli, Katerina

Published in:
Proceedings of the sixteenth IFIP WG 7.5 Working Conference

Publication date:
2012

Fragility curves for bridges under differential support motions

K. Konakli
Technical University of Denmark

ABSTRACT: This paper employs the notion of fragility to investigate the seismic vulnerability of bridges subjected to spatially varying support motions. Fragility curves are developed for four highway bridges in California with vastly different structural characteristics. The input in this analysis consists of simulated ground motion arrays with temporal and spectral nonstationarities, and consistent with prescribed spatial variation patterns. Structural damage is quantified through displacement ductility demands obtained from nonlinear time-history analysis. The potential use of the 'equal displacement' rule to approximately evaluate displacement demands from analysis of the equivalent linear systems is examined.

1 INTRODUCTION

For a structural component or system of interest, seismic fragility represents the probability that the demand imposed by earthquake loading will exceed a prescribed threshold, conditioned on a measure of ground motion intensity. The notion of fragility has been used widely to convey probabilistic information on seismic related damage (e.g., Kennedy & Ravindra 1984, Singhal & Kiremidjian 1996, Straub & Der Kiureghian 2008). Empirical fragility curves are developed using actual damage information from past earthquakes, whereas analytical fragility curves are based on simulation of structural response to seismic excitation. Existing models of analytical fragility curves for bridges (e.g. Shinozuka et al. 2000, Karim & Yamazaki 2001, Gardoni et al. 2003, Nielson & DesRoches 2007) vary as to the types of bridge structures examined, the characteristics of the considered input excitations, the selected measures of structural damage and ground motion intensity and the employed analysis methods. The vast majority of these studies assume uniform support motions; however, ground motion spatial variability may have significant influence on bridge response (Konakli & Der Kiureghian 2011).

Fragility curves for bridges subjected to differential support motions have been developed by considering stationary input (Lupoi et al. 2005) or by accounting for temporal nonstationarity in ground motions simulated with the spectral representation method (Deodatis et al. 2000, Saxena et al. 2000, Kim & Feng, 2003). In the aforementioned method, iterations required to match the target response spectra may alter the coherency characteristics of the initially generated ground motion arrays that are consistent with the assumed spatial variation pattern (Saxena et al. 2000). Furthermore, with the exception of Kim & Feng (2003) who considered several measures of ground motion intensity, fragility curves incorporating effects of spatial variability have been developed as functions of Peak Ground Acceleration (PGA), which may be a poor measure of the ground motion damage potential, as demonstrated subsequently in this paper.

In the current study, spatially varying support motions with temporal and spectral nonstationarities are simulated with the method developed by Konakli & Der Kiureghian (2012). This method extends earlier works by Vanmarcke & Fenton (1991) and Liao & Zerva (2006), and generates ground motion arrays that incorporate effects of *wave passage*, representing the time delay in the arrival of seismic waves at separate locations; *incoherence*, represent-

ing random differences in the amplitudes and phases of seismic waves at separate locations, caused by reflections and refractions and/or by the differential superpositioning of waves originating from an extended source; and differential *site response*, representing variations in the amplitudes and frequency contents of the surface motions, caused by propagation of the bedrock motions through varying soil profiles. Comparisons between coherency estimates from simulated arrays with the respective target coherency models demonstrate excellent agreement (Konakli & Der Kiureghian 2012). Preliminary investigations indicate higher correlation of structural damage with Spectral Acceleration (SA) than with PGA; thus, SA is used to characterize ground motion intensity. Pier displacement demands are evaluated with nonlinear time-history analysis. The potential use of the 'equal displacement' rule to approximately evaluate inelastic demands from analyses of the corresponding elastic systems is also examined.

2 BRIDGE MODELS

Fragility curves are developed for four highway bridges designed by the California Department of Transportation (Caltrans). These are prestressed concrete box-girder bridges that vary as to the number and length of spans, the configuration of the bents and the overall stiffness.

Idealized models of the bridges are shown in Figure 1. The Penstock Bridge is a four-span bridge with a single pier per bent. The deck has a vertical grade, varying from 0.3% to 2.1%, and a constant horizontal curvature of radius R = 458m. The columns are rigidly connected to the deck at the top and fixed in all directions at the bottom. The South Ingram Slough Bridge is a two-span bridge with two piers per bent. The deck has a vertical grade, varying from −0.52% to −0.85%, and a constant horizontal curvature of radius R = 1542.3m. The columns are rigidly connected to the deck at the top and fixed in all directions at the bottom. The Big Rock Wash Bridge is a three-span bridge with three piers per bent. The longitudinal axis of the bridge is a straight line. The deck is characterized by a constant profile grade of 0.5%. The piers are rigidly connected to the deck at the top, whereas the bottom supports are fixed in all translational directions and free in all rotational directions. The Auburn Ravine Bridge is a six-span bridge with two piers per bent. The deck has a vertical grade of 0.3% and a horizontal curvature of radius R = 1616m. The piers are rigidly connected to the deck at the top, whereas the bottom supports are fixed in all translational directions and free in all rotational directions. The ends of all four bridges are supported on seat abutments. The abutment response is modeled through two horizontal translational springs, whereas vertical translations are fully constrained.

Following Caltrans recommendations, 3 elements per pier are used in the finite element models. The number of elements in each span varies according to the span length. Condensing out rotational degrees of freedom (DOF), the resulting number of translational unconstrained DOF is 103 for the Penstock Bridge, 55 for the South Ingram Slough Bridge, 89 for the Big Rock Wash Bridge and 163 for the Auburn Ravine Bridge.

In linear elastic analysis, the flexural stiffness of the pier elements is the effective stiffness obtained from moment-curvature analysis. No stiffness reduction is required for the deck elements. The fundamental periods of the corresponding bridge models are 2.38s for the Penstock Bridge, 1.24s for the South Ingram Slough Bridge, 0.61s for the Big Rock Wash Bridge and 0.59s for the Auburn Ravine Bridge.

The nonlinear models differ from the corresponding elastic models only in the representation of the piers. These are modeled with force-based nonlinear elements with distributed plasticity. For the piers of the Penstock Bridge and the South Ingram Slough Bridge, 5 integration points along each element are defined, whereas for the shorter piers of the Big Rock Wash Bridge and the Auburn Ravine Bridge, the number of integration points per element is 3. For all four bridges, the cross-sections of the pier elements are modeled as fiber sections with 12 subdivisions in the circumferential direction and 8 and 4 subdivisions in the radial direction for the core and the cover, respectively. The reinforcing steel bars are specified as additional layers. The properties of the unconfined concrete and the reinforcing steel are the expected material properties defined by Caltrans specifications, whereas the properties of the confined concrete are determined according to Mander's model. The fiber model of the pier section accounts for interaction between axial force and bending moment. The shear and torsional behaviors are described by aggregated

uniaxial models with the shear yield force determined from Caltrans recommendations and the torsional yield force evaluated from theory of strength of materials.

Rayleigh damping is considered with the parameters adjusted so that the damping ratios of the lower modes are close to 5%.

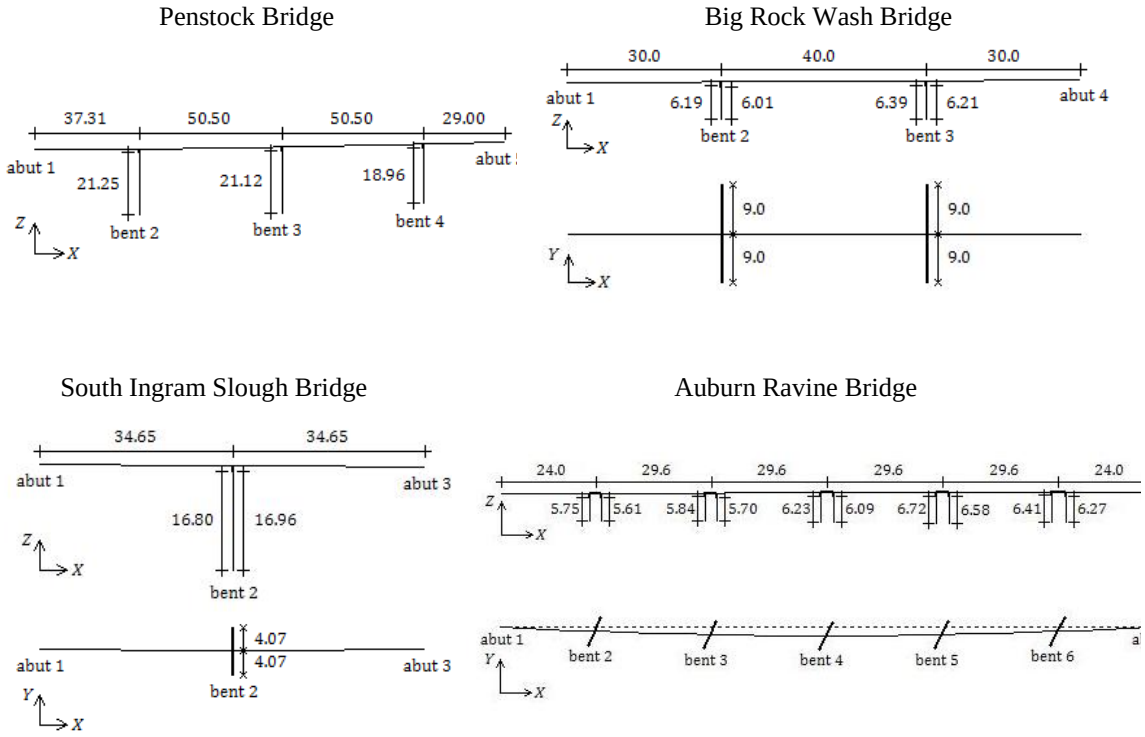

Figure 1. Bridge models.

3 INPUT EXCITATIONS

Synthetic ground motion arrays are generated with the method developed in Konakli & Der Kiureghian (2012). This method requires specification of a seed accelerogram at a reference location, a coherency function that describes the spatial variability of the ground motion random field in the frequency domain, and the Frequency Response Functions (FRF) of the soil columns underneath the bridge supports. The unconditional approach of this method, employed herein, simulates arrays of motions with uniform variability at all support points.

Two seed accelerograms are considered in this study; the fault-normal (FN) components of the Hollister South & Pine (HSP) record from the 1989 Loma Prieta earthquake and of the Pacoima Dam (PUL) record from the 1971 San Fernando earthquake. By using recorded accelerograms as seeds, the simulated motions inherit temporal and spectral characteristics of real earthquake motions. To achieve nonlinear bridge response, the HSP record is scaled with a factor of 1.5. (No scaling is applied to the stronger PUL record.) The corresponding acceleration time histories are shown in Figure 2.

The coherency between the ground acceleration processes at two sites, *k* and *l*, as a function of frequency, ω, is given by (Der Kiureghian 1996)

$$\gamma_{kl}(\omega) = |\gamma_{kl}(\omega)|^{incoherence} \exp\left\{i\left[\theta_{kl}(\omega)^{wave\ passage} + \theta_{kl}(\omega)^{site\ response}\right]\right\} \quad (1)$$

in which $|\gamma_{kl}(\omega)|^{incoherence} = \exp[-(\alpha d_{kl}\omega / v_s)^2]$ describes the incoherence component (Luco & Wong 1986), $\theta_{kl}(\omega)^{wave\ passage} = -\omega d_{kl}^{L} / v_{app}$ is the phase shift due to the wave-passage effect, and $\theta_{kl}(\omega)^{site\ response} = \tan^{-1}\{\mathrm{Im}[h_k(\omega)h_l(-\omega)] / \mathrm{Re}[h_k(\omega)h_l(-\omega)]\}$ is the phase shift due to the

site-response effect. In these expressions, α is an incoherence parameter, d_{kl} is the distance between supports k and l, v_s is the shear wave velocity of the ground medium, d_{kl}^L is the projected horizontal distance in the longitudinal direction of wave propagation, v_{app} is the surface apparent wave velocity, and $h_s(\omega)$, $s = k, l$, is the FRF for the absolute acceleration response of the site associated with the sth support DOF. In the current example, $h_s(\omega)$ is described by the FRF of the single-degree-of-freedom oscillator.

For all bridges, it is assumed that waves propagate in the direction from abutment 1 to the abutment at the other end of the bridge. Four cases of spatial variability are considered: case 1 is uniform support excitations; cases 2 and 3 incorporate effects of incoherence and wave passage, and represent two different levels of incoherence, $a = 0.2$ and $a = 0.4$, respectively; case 4 is case 2 plus site-response effects. For each bridge, the excitation in case 1 is the motion at a reference support from the corresponding array in case 2. The reference supports are bent 3 for the Penstock Bridge, bent 2 for the South Ingram Slough Bridge, bent 2 for the Big Rock Wash Bridge and bent 4 for the Auburn Ravine Bridge. In cases 2-4, the parameter values $v_s = 600$m/s and $v_{app} = 400$m/s are adopted. In case 4, the assumed variation of firm (F), medium (M) and soft (S) soil types at the supports from left to right is FMSMF for the Penstock Bridge, FSF for the South Ingram Slough Bridge, FMSF for the Big Rock Wash Bridge and FMSMSMF for the Auburn Ravine Bridge. For each of the cases 1-4 with the HSP record as seed, and 1-2 with the PUL record as seed, 20 support motion arrays are generated. These motions are applied as transverse excitations.

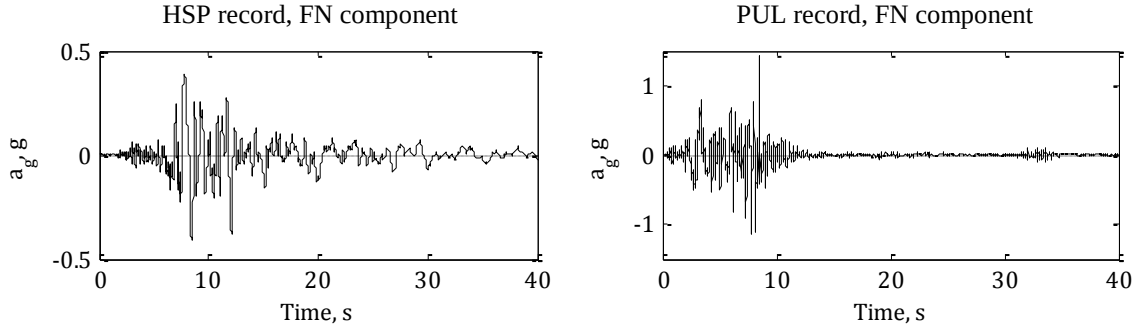

Figure 2. Acceleration time histories of seed records.

4 FRAGILITY ANALYSIS

Using a common convention, fragility curves are described by lognormal cumulative distribution functions (CDF). The parameters of the lognormal distribution are evaluated with the maximum likelihood method: Let I_k and D_k denote the values of the ground motion intensity and demand measures, respectively, in the kth simulation. Let D_{ref} denote the threshold value of the demand measure that defines 'failure'. Adopting the approach by Shinozuka et al. (2000), the kth simulation is considered a realization of a Bernoulli experiment with possible outcomes '1' or '0' depending on whether D_k exceeds D_{ref} or not. The probability of the outcome '1' at the kth trial is given by $F(I_k) = \Phi[\ln(I_k / c)/\zeta]$, in which F denotes the fragility function, Φ is the standard normal CDF, and c and ζ are the parameters of the lognormal distribution (median and log-standard deviation, respectively) to be estimated.

In the following analysis, damage is quantified through the displacement ductility factors of the piers, denoted μ. These factors are defined as the ratios of the maximum pier drifts evaluated from nonlinear time-history analysis to the corresponding yield drifts. The yield drifts are obtained from double integration of the curvature along the pier height, assuming that the section with the largest curvature has just yielded. The yield curvature is determined from moment-curvature analysis at section level. Each of the four bridges examined herein has piers with identical cross-sections and thus, identical yield curvatures.

A preliminary analysis is performed to select the ground motion intensity measure between the typically used PGA and SA. For each bridge and for all simulations in case 2, Figure 3 shows the maximum ductility factor among all piers, μ, versus PGA in the left graphs, and ver-

sus SA in the right graphs. Since PGA and SA vary among the bridge supports, the mean values over all support points are plotted. This figure clearly indicates a higher correlation of damage with SA, which is adopted as the ground motion intensity measure in the following analysis. (Similar observations were made for the other cases of spatial variability examined in this study.) In Gardoni et al. (2003), the appropriateness of SA to characterize ground motion intensity has been demonstrated as a result of a step-wise deletion process.

Accounting for the ranges of ductility factors obtained in the simulations, the threshold values that define failure are selected as $\mu_{ref} = 2$ for the Penstock Bridge, $\mu_{ref} = 2$ for the South Ingram Slough Bridge, $\mu_{ref} = 3$ for the Big Rock Wash Bridge and $\mu_{ref} = 2$ for the Auburn Ravine Bridge. Each bridge is considered a series system, i.e., failure occurs when μ_{ref} is exceeded for at least one pier. The estimated medians and log-standard deviations of the fragility functions are listed in Table 1. The corresponding curves are shown in Figure 4: The graphs on the left show fragility curves for cases 1-4 with the HSP record as seed, and thus, demonstrate effects of different spatial variation patterns. The graphs on the right show fragility curves for cases 1-2 for both HSP and PUL, and thus, demonstrate sensitivities with respect to the characteristics of the seed record. For both seeds, effects of spatial variability are mild on the Penstock Bridge and the South Ingram Slough Bridge, i.e., on the two more flexible bridges, and are more pronounced on the stiffest Auburn Ravine Bridge. The latter is less vulnerable to spatially varying support motions than to uniform motions. The opposite trend, i.e. increased seismic vulnerability due to spatial variability of the support motions, has been reported in other studies (Deodatis et al. 2000, Saxena et al. 2000, Kim & Feng, 2003, Lupoi et al. 2005). Differences in the approaches of those studies versus the approach employed herein are mentioned in the Introduction.

Computational cost as well as convergence and stability problems are main drawbacks in the nonlinear time-history analysis approach. Consideration of spatial variations in the input poses additional challenges by further complicating the system of nonlinear equations to be solved. Therefore, approximate simplified analysis methods are of major interest. On the basis of the 'equal displacement' rule (Veletsos and Newmark, 1960), displacement demands computed for the linear structure can be used to approximate the inelastic displacement demands as long as the fundamental period of the structure is larger than the predominant period of the site. In Caltrans design practice, the 'equal displacement' rule is adopted for bridges with fundamental periods within the range 0.7s and 3s. Table 2 lists the medians of the lognormal distributions describing the fragility curves estimated with the same approach as before, but with the displacement demands computed from linear time-history analysis. The numbers in the parentheses are the ratios of these approximate median estimates to the medians listed in Table 1. These ratios demonstrate trends consistent with results from analyses under uniform excitations: Approximations of the 'equal displacement' rule tend to be slightly conservative for 'sufficiently flexible' structures (Gupta and Krawinkler 2000) and depend on ductility factors for structures with lower fundamental periods (Vidic et al. 1994).

Table 1. Medians (in units of *g*) of fragility curves. (The numbers in parentheses are the corresponding log-standard deviations.)

Bridge name	HSP case 1	HSP case 2	HSP case 3	HSP case 4	PUL case 1	PUL case 2
Penstock	0.36 (0.17)	0.34 (0.18)	0.38 (0.03)	0.38 (0.12)	0.33 (0.11)	0.33 (0.11)
S. Ingram Slough	0.87 (0.00)	0.91 (0.13)	0.85 (0.07)	0.85 (0.09)	0.85 (0.00)	0.89 (0.00)
Big Rock Wash	0.37 (0.30)	0.44 (0.11)	0.44 (0.13)	0.44 (0.19)	0.73 (0.25)	0.83 (0.21)
Auburn Ravine	1.01 (0.11)	1.65 (0.32)	1.26 (0.11)	2.76 (0.94)	0.86 (0.20)	1.13 (0.43)

Table 2. Medians (in units of *g*) of fragility curves obtained with the 'equal displacement' rule. (The numbers in parentheses are the ratios of the medians in Table 2 to the medians in Table 1.)

Bridge name	HSP case 1	HSP case 2	HSP case 3	HSP case 4	PUL case 1	PUL case 2
Penstock	0.32 (0.89)	0.28 (0.82)	0.30 (0.79)	0.31 (0.82)	0.35 (1.06)	0.29 (0.88)
S. Ingram Slough	0.70 (0.80)	0.80 (0.88)	0.80 (0.94)	0.77 (0.91)	0.75 (0.88)	0.75 (0.84)
Big Rock Wash	0.41 (1.11)	0.45 (1.02)	0.40 (0.91)	0.41 (0.93)	0.79 (1.08)	0.76 (0.92)
Auburn Ravine	0.87 (0.86)	1.07 (0.65)	1.19 (0.94)	1.30 (0.47)	0.78 (0.91)	0.75 (0.66)

5 CONCLUSIONS

Effects of ground motion spatial variability on seismic fragilities were investigated for four highway bridges in California. Arrays of ground motions with temporal and spectral nonstationarities, and consistent with prescribed spatial variation patterns, were used as input. Damage was quantified through pier displacement ductility factors, evaluated from nonlinear time-history analyses. Effects of spatial variability were more pronounced for the stiffest among the bridges; for this bridge, spatial variations decreased seismic vulnerability. Approximations of the 'equal displacement' rule demonstrated trends similar to those reported in literature for the case of uniform excitations.

6 REFERENCES

Deodatis, G., Saxena, V., & Shinozuka, M., 2000. Effect of spatial variability of ground motion on bridge fragility curves. *Proceedings of the 8th ASCE Specialty Conference on Probabilistic Mechanics and Structural Reliability*, University of Notre Dame.

Der Kiureghian, A., 1996. A coherency model for spatially varying ground motions. *Earthquake Engineering and Structural Dynamics* 25: 99-111.

Gardoni, P., Mosalam, K.M., & Der Kiureghian, A., 2003. Probabilistic seismic demand models and fragility estimates for RC bridges. *Journal of Earthquake Engineering* 7 (Special Issue 1): 79-106.

Gupta, A., & Krawinkler, H., 2000. Estimation of seismic drift demands for frame structures. *Earthquake Engineering and Structural Dynamics* 29: 1287-1306.

Karim, K.R., & Yamazaki, F., 2001. Effect of earthquake ground motions on fragility curves of highway bridge piers based on numerical simulation. *Earthquake Engineering and Structural Dynamics* 30:1839-1856.

Kennedy, R.P., & Ravindra, M.K., 1984. Seismic fragilities for nuclear power plant risk studies. *Nuclear Engineering and Design* 79: 47-68.

Kim, S., & Feng, M.Q. 2003. Fragility analysis of bridges under ground motion with spatial variation. *International Journal of Non-Linear Mechanics* 38: 705-721.

Konakli, K., & Der Kiureghian., A., 2011. Stochastic dynamic analysis of bridges subjected to spatially varying ground motions. *Report No. 2011/105*, Pacific Earthquake Engineering Research Center, University of California, Berkeley.

Konakli, K., & Der Kiureghian, A., 2012. Simulation of spatially varying ground motions including incoherence, wave-passage and site-response effects. *Earthquake Engineering and Structural Dynamics* 41: 495-513.

Liao, S., & Zerva, A., 2006. Physically compliant, conditionally simulated spatially variable seismic ground motions for performance-based design. *Earthquake Engineering and Structural Dynamics* 35: 891-919.

Luco, J.E., & Wong, H.L., 1986. Response of a rigid foundation to a spatially random ground motion. *Earthquake Engineering and Structural Dynamics* 14: 891-908.

Lupoi, A., Franchin, P., Pinto, P.E., & Monti, G. Seismic design of bridges accounting for spatial variability of ground motion, 2005. *Earthquake Engineering and Structural Dynamics* 34: 327-348.

Nielson, B.G., & DesRoches, R., 2007. Seismic fragility methodology for highway bridges using a component level approach. *Earthquake Engineering and Structural Dynamics* 36: 823-839.

Saxena, V., Deodatis, G., Shinozuka, M., & Feng, M.Q., 2000. Development of fragility curves for multi-span reinforced concrete bridges. *Proceedings of the International Conference on Monte Carlo Simulation*, Principality of Monaco.

Shinozuka, M., Feng, M.Q., Lee, J., & Naganuma, T., 2000. Statistical analysis of fragility curves. *Journal of Engineering Mechanics* 126(12): 1224-1231.

Singhal, A., & Kiremidjian, A.S., 1996. Method for probabilistic evaluation of seismic structural damage. *Journal of Structural Engineering* 122(12): 1459-1467.

Straub, D., & Der Kiureghian, A., 2008. Improved seismic fragility modeling from empirical data. *Structural Safety* 30: 320-336.

Vanmarcke E.H., & Fenton G.A., 1991. Conditioned simulation of local fields of earthquake ground motion. *Structural Safety* 10: 247-264.

Veletsos, A.S., & Newmark, N.M., 1960. Effect of inelastic behavior on the response of simple systems to earthquake motions. *Proceedings of the 2nd World Conference on Earthquake Engineering*, Japan, 2:895-912.

Vidic, T., Fajfar, P., & Fischinger, M., 1994. Consistent inelastic design spectra: strength and displacement. *Earthquake Engineering and Structural Dynamics* 23: 502-521.

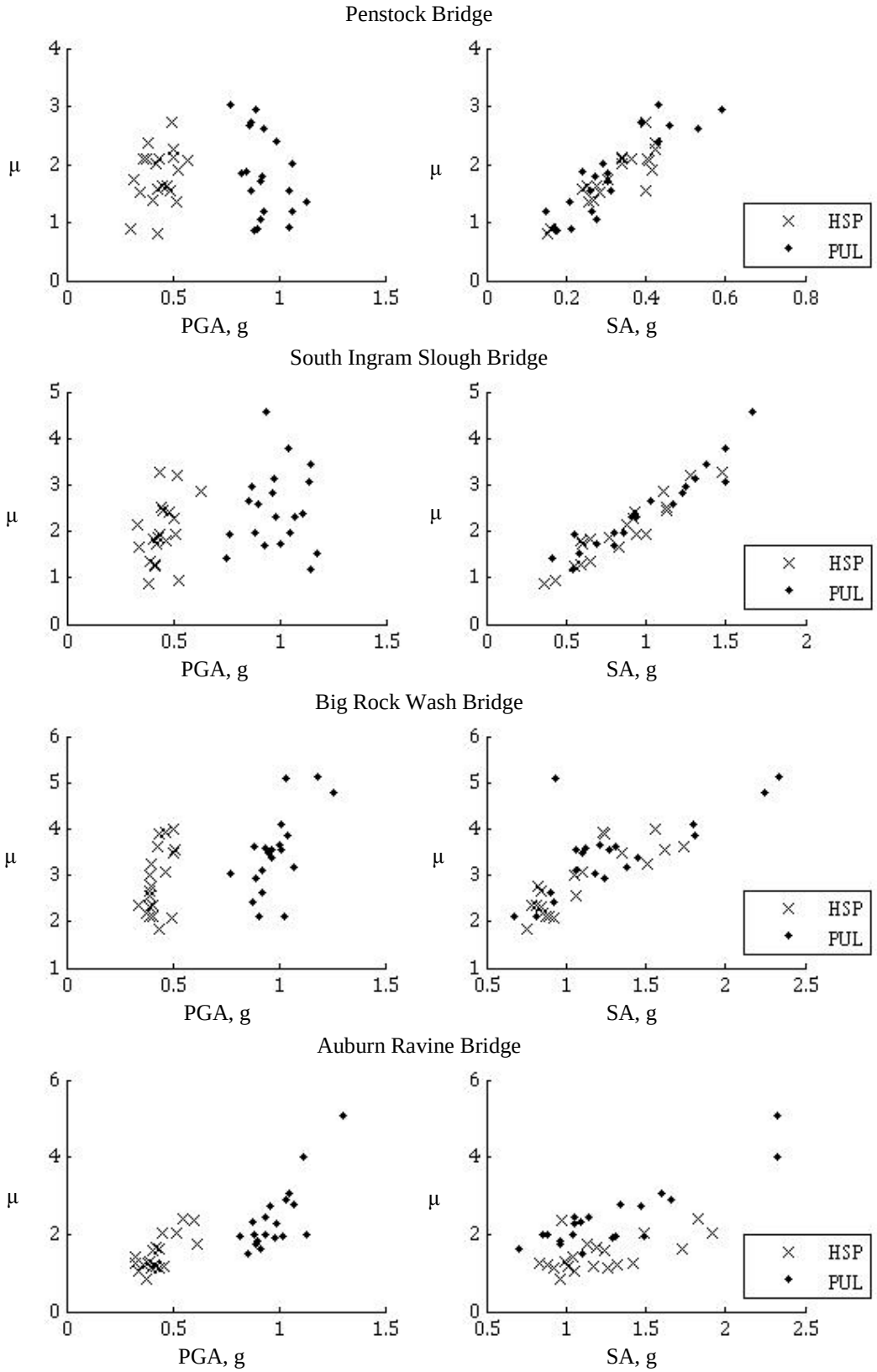

Figure 3. Maximum displacement ductility factors versus PGA (left graphs) and versus SA (right graphs).

Penstock Bridge

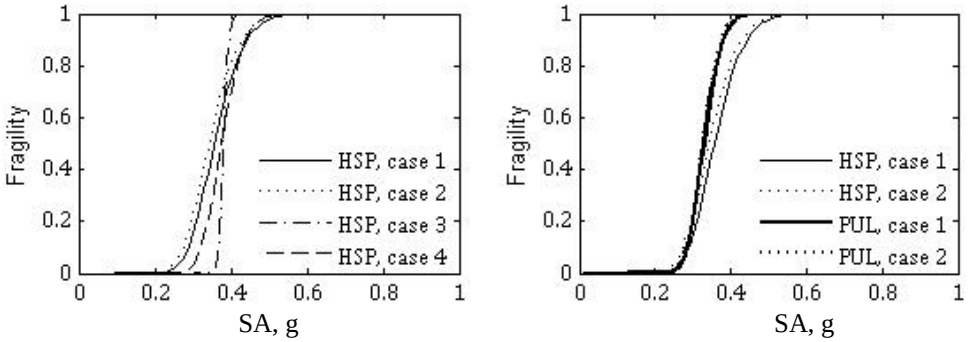

South Ingram Slough Bridge

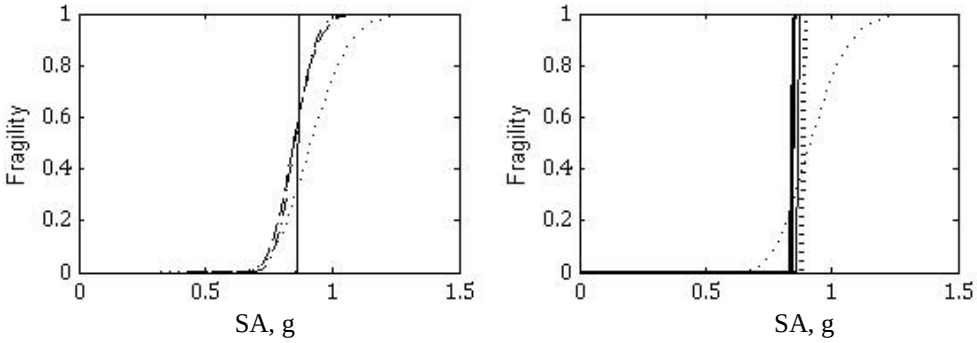

Big Rock Wash Bridge

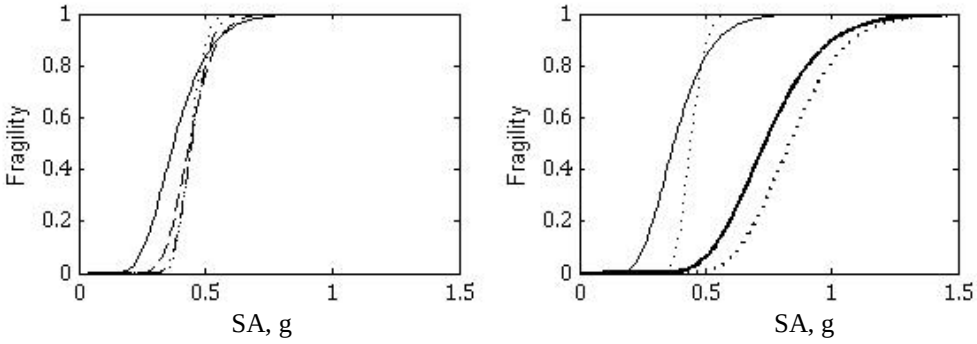

Auburn Ravine Bridge

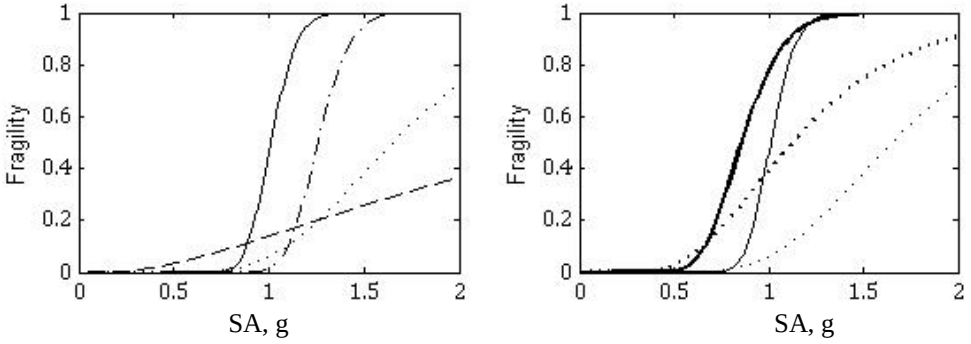

Figure 4. Fragility curves.